Applied Catalysis B: Environmental 94 (2010) 150–157

Contents lists available at ScienceDirect

Applied Catalysis B: Environmental

journal homepage: www.elsevier.com/locate/apcatb

# Highly active $WO_3$ semiconductor photocatalyst prepared from amorphous peroxo-tungstic acid for the degradation of various organic compounds

Kazuhiro Sayama [a,*], Hiroki Hayashi [a,b], Takeo Arai [a], Masatoshi Yanagida [a], Takahiro Gunji [a,b], Hideki Sugihara [a]

[a] Energy Technology Research Institute, National Institute of Advanced Industrial Science and Technology (AIST), Central 5, 1-1-1 Higashi, Tsukuba, Ibaraki 305-8565, Japan
[b] Graduate School of Science and Technology, Tokyo University of Science, 2641 Yamasaki, Noda, Chiba 278-8514, Japan

ARTICLE INFO

*Article history:*
Received 13 August 2009
Received in revised form 2 November 2009
Accepted 3 November 2009
Available online 20 November 2009

*Keywords:*
$WO_3$
Semiconductor
Photocatalyst
Degradation

ABSTRACT

The photocatalytic activity and physical properties on $WO_3$ photocatalysts prepared by various methods were investigated. $WO_3$ photocatalyst ($WO_3$(PA)) prepared from aged amorphous peroxo-tungstic acid showed the highest activity for hexane degradation, which was ~6 times higher than that of commercial $WO_3$, and exhibited a strong absorption in visible light region. $WO_3$(PA) loaded with CuO as co-catalyst showed a high activity for the complete oxidation of various organic compounds into $CO_2$, as compared with the activities of commercial or homemade $WO_3$ catalysts and N-doped $TiO_2$. The high activity of $WO_3$(PA) was explained by high surface area, good crystallinity, and efficient light absorption in visible light region. The light absorption of $WO_3$(PA) powder was probably improved because of a decrease in surface reflection at the smooth and porous surface of $WO_3$(PA) and because of its increased light path length.



## 1. Introduction

Visible-light-responsive photocatalysts have been extensively investigated for indoor applications. Various $TiO_2$ photocatalysts doped with anions (N, S, C, etc.) and complicated semiconductor photocatalysts using mixed metal oxides have been developed [1–5] for the degradation of harmful organic substances such as volatile organic compounds (VOCs); however, the photocatalytic activities of these complicated composites are not sufficient for practical use. On the other hand, tungsten oxide ($WO_3$) is a visible-light-responsive photocatalyst that absorbs light up to ca. 480 nm. Compared with mixed metal oxides and doped oxides, $WO_3$ is easy to prepare, modify, and use to coat substrates. $WO_3$ also is harmless and is stable in acidic and oxidative conditions. However, very few reports exist concerning the degradation of organic substances over $WO_3$ photocatalysts a little while ago [6–9], because this material's photocatalytic activity toward organic substances is very low without any suitable co-catalysts. Furthermore, the complete oxidation of organic substances to $CO_2$ (complete mineralization) over these $WO_3$ photocatalysts has not been investigated. Very recently, it is reported that the activity of $WO_3$ photocatalysts for the complete oxidation of VOCs could be improved significantly in the presence of suitable co-catalysts such as Pt, Pd, and Cu compounds, as well as $Cu^{2+}$ ions [10–19]. The activities of $WO_3$ photocatalysts observed under visible or fluorescent light in the presence of these co-catalysts were higher than those of $TiO_2$-based photocatalysts [11–15,19].

Most of the reported $WO_3$ photocatalyst studies to date have employed commercially available $WO_3$ powders. The surface areas of most of these commercialized $WO_3$ powders are very low (3–7 $m^2/g$) compared with the surface area of $TiO_2$ (a few dozens to a few hundreds $m^2/g$). Surface area is generally one of the important factors that affects photocatalytic activity. Here, we investigated various methods for preparing $WO_3$ semiconductors with various surface areas (1–53 $m^2/g$) to improve photocatalytic activity and to clarify the relationship between the activity and the surface area of $WO_3$. On the way of this investigation, we found that $WO_3$ prepared from amorphous peroxo-tungstic acid (PA) showed a high activity for the degradation of various organic compounds, and this $WO_3$ powder exhibited efficient absorption in visible light region. This efficient light absorption appeared to cause increased photocatalytic activity and to reduce the amount of photocatalyst required for practical applications. The reasons for the observed high activity and for the efficient light absorption of $WO_3$ prepared from amorphous peroxo-tungstic acid are discussed in this report.

## 2. Experimental

Two kinds of $WO_3$ powders (referred to as $WO_3$(PA) and $WO_3$(C)) were prepared from W metal and $H_2O_2$. W metal powder

* Corresponding author. Tel.: +81 29 8616234; fax: +81 29 8614760.
*E-mail address:* k.sayama@aist.go.jp (K. Sayama).

0926-3373/$ – see front matter © 2009 Elsevier B.V. All rights reserved.
doi:10.1016/j.apcatb.2009.11.003

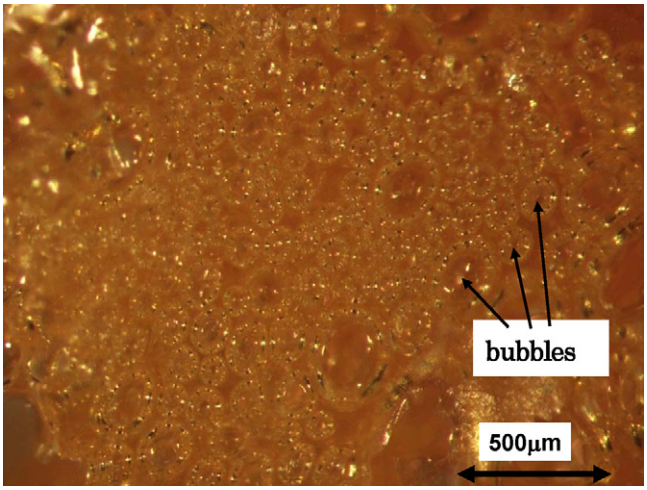


**Fig. 1.** Photograph of a-PA powder before calcination acquired by means of an optical microscope.

(0.0226 mol, Araido Material Co.) was completely dissolved in aqueous $H_2O_2$ (0.507 mol, 30%, Wako Chemical Co.) in a glass beaker, and the transparent colorless solution was evaporated quickly on a hot stirplate. The white powder remaining in the beaker after evaporation was crystalline peroxo-tungstic acid, $[WO_2(O_2)H_2O]\cdot nH_2O$ [20]. $WO_3$(C) powder was prepared by calcination of crystalline $[WO_2(O_2)H_2O]\cdot nH_2O$ at 400–700 °C (standard and maximum activity: 400 °C) in air for 30 min. To prepare $WO_3$(PA) powder, $[WO_2(O_2)H_2O]\cdot nH_2O$ (5.15 g) was dissolved again in hot water (100 ml), and the solution temperature was kept at ca. 70 °C for 90 min on a hot stirplate to age the solution. The colorless solution became orange during this aging treatment, and then gradually evaporated. During evaporation, the viscosity of the orange solution increased, and bubbles of $O_2$ gas were observed in the viscid gel. As these $O_2$ bubbles burst, an amorphous orange peroxo-tungstic acid powder evolved from the gel, $WO_3\cdot xH_2O_2\cdot yH_2O$ ($0.05 < y < 1$) [21]. This amorphous powder is referred to herein as "a-PA". Fig. 1 shows the large particle of a-PA observed by an optical microscope. There are many bubbles with sizes of a few μm to 200 μm inside the a-PA particle. $WO_3$(PA) powder then was prepared by calcination of the a-PA powder at 400–700 °C (standard and maximum activity: 450 °C) in air for 30 min. The a-PA large powder was naturally shattered during the calcination due to the burst of bubbles inside the a-PA, and became $WO_3$(PA) fine powder. $WO_3$(PA) powder was used without any additional crushing. In some cases, $WO_3$(PA) was ground mechanically, that was crushed manually in a mortar for ca. 5 min, is referred to here as $WO_3$(PA-g). Mesoporous $WO_3$ was prepared from $WCl_6$ in ethanol with poly(alkylene oxide) triblock copolymer (P103 Adeka Pluronic, $EO_{20}PO_{70}EO_{20}$) as a template, as reported previously [22]. A simple homemade $WO_3$ powder was also prepared by calcination of $H_2WO_4$ powder. Commercial $WO_3$ powder (99.99%, surface area: ca. 4 $m^2/g$) was obtained from Kojundo Chemical Lab. Co.; this powder was used in previous studies on $WO_3$ photocatalysts for various reactions such as VOC degradation [10,12,16,17] and water splitting [23,24]. For co-catalyst CuO loading, an impregnation method with $Cu(NO_3)_2$ aqueous solution was used, followed by calcination at 300 °C in air for 30 min. N-doped $TiO_2$, prepared as reported by Irokawa et al. [2], was used as the reference photocatalyst.

Photocatalytic degradation of organic substances was conducted in a glass vial (4.4 ml), in which a sufficient amount of $WO_3$ (150 mg) was used to completely cover the bottom (area: 1.1 $cm^2$). The vial was sealed with a septum cap for sampling, and then organic substances were introduced into the vial with a syringe.

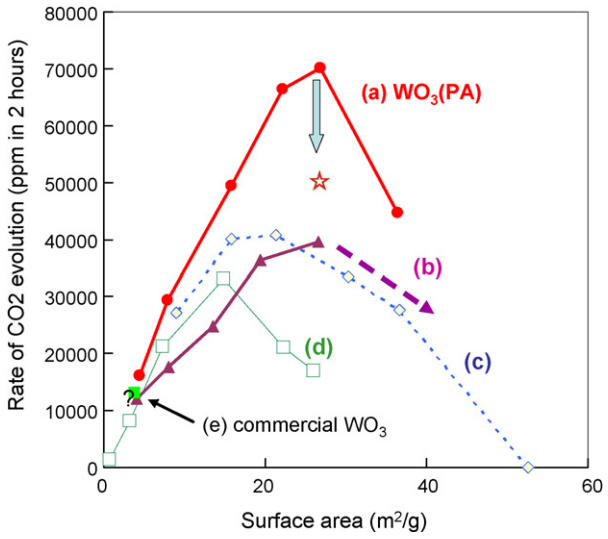


**Fig. 2.** The relationship between the $CO_2$ evolution rate for the degradation of hexane and the surface area of $WO_3$ prepared by various methods. (a) $WO_3$(PA), (b) $WO_3$(C), (c) mesoporous $WO_3$, (d) $WO_3$ prepared by calcining $H_2WO_4$, and (e) commercial $WO_3$. (*) $WO_3$(PA-g). Surface areas were varied by changing the calcination temperature. Experimental conditions: solar-simulating Xe light (1 sun) without UV cutoff filter; hexane: 2 μl.

The bottom of the vial was irradiated with light from a solar-simulating xenon lamp (CERMAX LX-300, with a half mirror to simulate AM-1.5 and 1 sun intensity at around 400–500 nm). The concentrations of $CO_2$ generated in the photocatalytic degradation of the organic substances were measured by a gas chromatograph (Shimadzu, GC-14B) with a flame ionization detector equipped with a methanizer. The absorbance (KM) of $WO_3$ powder was calculated from the measured reflectance by means of the Kubelka–Munk theory with Jasco, V-570 spectrometer software. The reflectance was measured with an integrating sphere. X-ray diffraction (XRD) pattern was measured using MX-Labo (Mac Science Co.).

## 3. Results and discussion

We varied the surface area and the extent of crystalline growth by changing the calcination temperature in each preparation

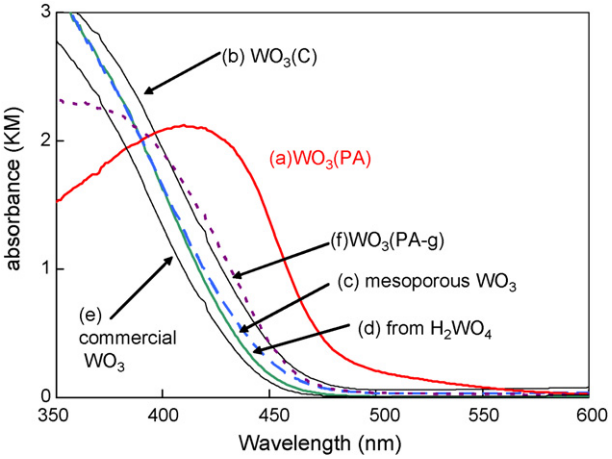


**Fig. 3.** UV–vis absorption spectra of various $WO_3$ samples. (a) $WO_3$(PA) calcined at 450 °C (22 $m^2/g$ surface area), (b) $WO_3$(C) calcined at 400 °C (27 $m^2/g$ surface area), (c) mesoporous $WO_3$ calcined at 450 °C (21 $m^2/g$ surface area), (d) $WO_3$ prepared by calcining $H_2WO_4$ at 400 °C (22 $m^2/g$ surface area), (e) commercial $WO_3$ (4 $m^2/g$ surface area), and (f) $WO_3$(PA-g) (23 $m^2/g$ surface area).

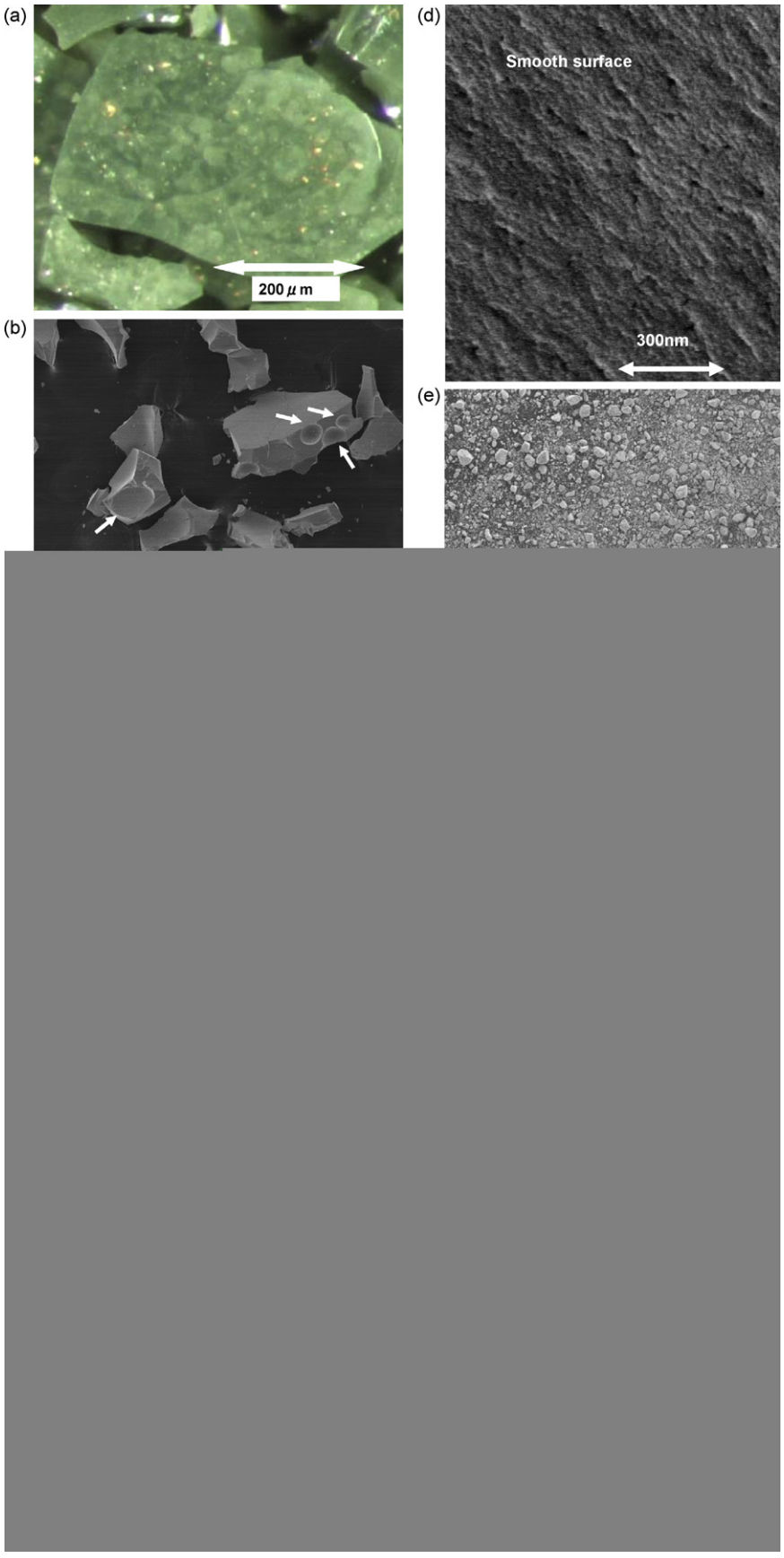


**Fig. 4.** Photographs of $WO_3$(PA) powder (calcined at 450 °C) acquired by means of an optical microscope (a) and a scanning electron microscope (b–d); (b) low magnification, (c) smooth surface and fracture cross-section, (d) high magnification, and (e–g) SEM photographs of $WO_3$(PA-g) powder after grinding at various magnifications.

method. The degradation of hexane, known as a typical VOC in gasoline, is reportedly very efficient on $WO_3$ powder without co-catalysts [13]. For catalyst screening tests, we first compared the hexane degradation activities of various $WO_3$ powders without co-catalyst to avoid the complicated influence of the loading condition of co-catalyst. The relationship between the $CO_2$ evolution rate for the degradation of hexane and the surface area of $WO_3$ prepared by various methods is shown in Fig. 2. The crystal phase of all $WO_3$ samples plotted in Fig. 2 was mainly monoclinic. The photocatalytic activity increased with increasing surface area; however, the activity decreased when the surface area was too large, and the optimum surface area appeared to be around 15–27 $m^2/g$ for each preparation method. It is surmised that as the surface area increased, the crystallinity of $WO_3$ worsened and the number of defects in the $WO_3$ crystal increased. $WO_3$(PA) exhibited the best activity among all the tested $WO_3$ samples. The activity of $WO_3$(PA) was clearly higher than that of $WO_3$(C), which was prepared from the same precursor of $WO_3$(PA) but did not undergo aging treatment. The maximum activity of $WO_3$(PA) calcined at 450 °C was ca. 6 times that of commercial $WO_3$. The surface area of mesoporous $WO_3$ prepared at 350 °C was very high (57 $m^2/g$), and the XRD pattern for this samples revealed a monoclinic phase. However, the photocatalytic activity of mesoporous $WO_3$ for $CO_2$ evolution was negligible. We speculate that this mesoporous $WO_3$ might have contained many defects, causing charge recombination to occur effectively at these defect sites.

$WO_3$(PA) had a unique light absorption spectrum compared with the other $WO_3$, samples (Fig. 3). Samples with similar surface areas (21–27 $m^2/g$. See caption in Fig. 3) and high photocatalytic activity were selected among these preparation methods. Except for $WO_3$(PA), the absorption spectra (Fig. 3b–d) of all the homemade $WO_3$ powders, including $WO_3$(C) and commercial $WO_3$ (Fig. 3e), decreased monotonously from the ultraviolet (UV) region to 480 nm, independent on the calcination temperature. In contrast, for $WO_3$(PA) (Fig. 3a), the absorption between 400 and 500 nm intensified substantially compared with the other $WO_3$ samples, suggesting that the light absorption band seemed to be red-shifted to longer wavelengths.

The particle size of as-prepared $WO_3$(PA) (i.e., without any additional crushing) was less than 200 μm on average. We measured the morphology of a relatively large particle with an optical microscope (Fig. 4a). The surface of all particles was very flat and smooth, and the color was transparent dark green. The light reflection was sometimes colorful, and red opalescent reflection spots were observed. Some opaque internal features, with sizes of a few μm to 50 μm, were observed beneath the transparent green surface layer (Fig. 4a). These internal features were probably bubbles, hollows, or aggregates of tightly packed primary particles with different refractive indexes. Fig. 4(b–d) shows SEM photographs of $WO_3$(PA) powder. Some semispherical hollows (white arrows in Fig. 4b) with sizes of 50–100 μm were observed on the otherwise very smooth surface. During the preparation of solid a-PA, a precursor of $WO_3$(PA), some bubbles of $O_2$ from the decomposition of peroxo species were taken up in the viscous orange liquid, and the solidified orange liquid of peroxo-tungstic acid (a-PA) was formed with $O_2$ bubbles, as shown in Fig. 1. Then, The a-PA large powder was naturally shattered during the calcination due to burst of large bubbles inside the a-PA, and became $WO_3$(PA) fine powder, while small bubbles might remain in the $WO_3$(PA) as small hollows. Therefore, we considered the semispherical hollows on the surface to be traces of middle size bubbles. The surface of the semispherical hollows was also very smooth, as were the other flat surfaces of the sample. The roughness of the surface was less than 40 nm (Fig. 4c and d), and primary particles and pores were hardly observed on the smooth surface by SEM observation; however, it is reasonable that very

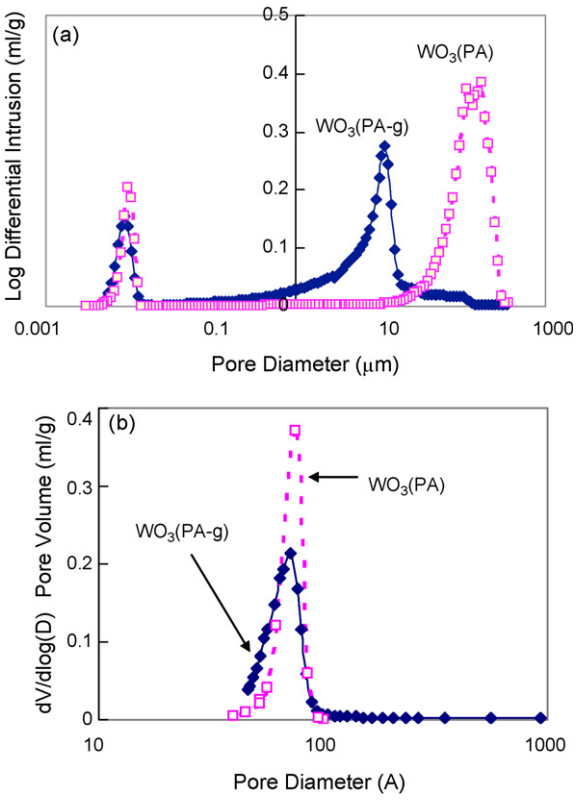


**Fig. 5.** The pore size distribution of $WO_3$(PA) and $WO_3$(PA-g) measured by (a) Hg filling method and by (b) $N_2$ adsorption–desorption method.

small pores to pass through the reactant gases or $N_2$ are present on the surface of the particles, since they had a large surface area (ca. 22 $m^2/g$) and the highest activity. Beneath the smooth surface of $WO_3$(PA), many particles of 30–40 nm diameter were observed, as shown in the SEM image of a fracture cross-section (Fig. 4c). Two peaks were observed in the pore size distribution of $WO_3$(PA) at around 8 nm and 180 μm, measured by Hg filling method, as shown in Fig. 5(a). After grinding of $WO_3$(PA), the former peak position at 8 nm was not changed, but latter peak was significantly shifted smaller to 10 μm and broadened. The latter large peak is mainly caused by the pores made by the interspaces of the large particles shown in Fig. 4(a and b). The results of the pore size distributions measured by $N_2$ adsorption–desorption method at around 8 nm (Fig. 5b) were almost similar to those by Hg filling method. The peak position around 8 nm was not changed, but it was slightly broadened after grinding. The small peak around 8 nm is caused by the pores made by the interspaces of the primary particles. Considering the markedly rough surface at the fracture cross-section (Fig. 4c) and the image obtained with the optical microscope (Fig. 4a), we surmised that some non-uniform small hollows (low density part) created by desorbing $H_2O$ and $O_2$ gases from the solid a-PA during heating, or some aggregates (high density part) of tightly packed primary particles, might be present inside the $WO_3$(PA) particles.

Figs. 6 and 7 show the absorption spectra and the SEM photographs of $WO_3$(PA) prepared at various temperatures, and the photocatalytic activity and various properties on $WO_3$(PA) photocatalysts are summarized in Table 1. The absorptions of all $WO_3$(PA) samples in visible light region were higher than that of normal $WO_3$. The absorption threshold of $WO_3$(PA) prepared at 700 °C was slightly shifted to the short wavelength region. The smooth surface morphology of $WO_3$(PA) observed by SEM was not changed up to 600°C, but growth of particles and pores were observed on the surface of $WO_3$(PA) calcined at 700 °C, as shown in

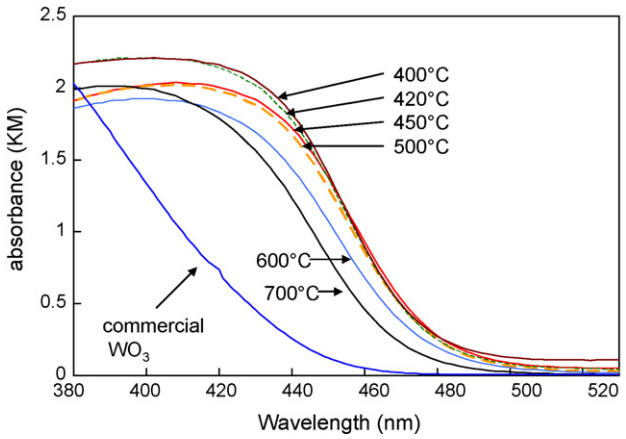


**Fig. 6.** UV–vis absorption spectra of various $WO_3$(PA) prepared at different temperature.

Fig. 7. The surface area was decreased and particle size was increased with increasing the calcination temperature. The increase of the roughness on the surface and the growth of particles probably affected the blue-shift of absorption spectra of $WO_3$(PA) calcined at 700 °C.

We ground the $WO_3$(PA) with a mortar to destroy its secondary structure, such as the smooth surface, aggregates, and hollows. This grounded powder is described as $WO_3$(PA-g), and only particles of 30–40 nm were observed by SEM measurement (Fig. 4f and g). Particles of 30–40 nm were the primary particles, which were also confirmed by calculation using the half-bandwidth of the corresponding XRD pattern. The surface area of $WO_3$(PA) (22 $m^2$/g) was slightly increased after grinding (23 $m^2$/g). Notably, the absorption spectra of $WO_3$(PA-g) powder (Fig. 3f) differed from that of $WO_3$(PA) powder (Fig. 3a) and was relatively similar to those of the other $WO_3$ powders. It is noted that the visible light absorption of the a-PA having smooth surface and internal bubbles was also significantly changed by destruction of the secondary structure using a mortar, as shown in Fig. 8. Therefore, we concluded that the secondary structures of the $WO_3$(PA) and a-PA samples were responsible for its unique absorption spectrum.

Furthermore, the destruction of the secondary structure by grinding also affected the photocatalytic activity. The data point (*) in Fig. 2 shows the photocatalytic activity of $WO_3$(PA-g), which was decreased about 28% compared to that of $WO_3$(PA). To investigate whether defects produced by grinding $WO_3$(PA) affected on the activity, $WO_3$(PA-g) was annealed at the same temperature as that used for the preparation of $WO_3$(PA); however, the activity was not changed by annealing. The activities and absorption spectra of other $WO_3$ samples hardly changed after grinding. When a-PA powder was ground and then calcined, an absorption spectrum and activity similar to those of $WO_3$(PA-g) were observed. The activities of $WO_3$(PA) and $WO_3$(PA-g) were almost the same under UV light irradiation with a black light. Therefore, the possibility, that the activity of $WO_3$(PA-g) was reduced by the formation of defects after grinding, is denied. The tailing of the absorption of $WO_3$(PA) around 500 nm was observed in Fig. 3(a), but it was disappeared after grinding. It is speculated that the small absorption originated from the defects of the primary particles around 500 nm was also intensified by the secondary structure of $WO_3$(PA).

**Table 1**
The photocatalytic activity of hexane degradation and various properties on $WO_3$(PA) prepared at different preparation temperature.

| Preparation temperature (°C) | Photocatalytic activity[a] (ppm/2 h) | Surface area ($m^2$/g) | Absorption threshold (nm) | Primary particle size[b] (nm) |
|---|---|---|---|---|
| 400 | 44,700 | 36 | 481 | 41 |
| 420 | 70,200 | 27 | 481 | 40 |
| 450 | 66,300 | 22 | 482 | 42 |
| 500 | 49,500 | 16 | 482 | 46 |
| 600 | 29,300 | 8 | 480 | 52 |
| 700 | 16,100 | 4 | 472 | 52 |

[a] The photocatalytic activity of hexane degradation.
[b] It was estimated by full width at half maximum of XRD measurement.

Fig. 9 shows the action spectra of the apparent quantum efficiency of $CO_2$ formation from hexane using monochromatic light. The apparent quantum efficiency over $WO_3$(PA) was ca. 7% at 450 nm, and it was higher than that over $WO_3$(PA-g). The shapes of the action spectra in Fig. 9 and absorption spectra in Fig. 3 on $WO_3$(PA) and $WO_3$(PA-g) were similar to each other. The quantum efficiency was reduced only in visible light region by grinding, while that at 400 nm was not reduced. Therefore, we concluded that the main reason for the higher activity of $WO_3$(PA) relative to that of $WO_3$(PA-g) was the higher light absorption capacity of $WO_3$(PA).

Next, we investigated the photocatalytic activity of $WO_3$ loaded with CuO co-catalyst. In the case of the degradation of acetaldehyde, malodorous substance in tobacco smoke, the complete oxidation into $CO_2$ gas (18,000 ppm) of acetaldehyde (9000 ppm) could take place over CuO(0.1 wt%)–$WO_3$(PA), and the activity decreased by ca. 30% after grinding. Fig. 10 shows the time course of $CO_2$ formation during the degradation of propane over various $WO_3$ loaded with CuO co-catalyst and over N-doped $TiO_2$. CuO-loaded $WO_3$(PA) oxidized propane (ca. 22,700 ppm) completely and effectively into $CO_2$ (ca. 68,000 ppm). The activity over $WO_3$(PA) without CuO co-catalyst gradually decreased, because

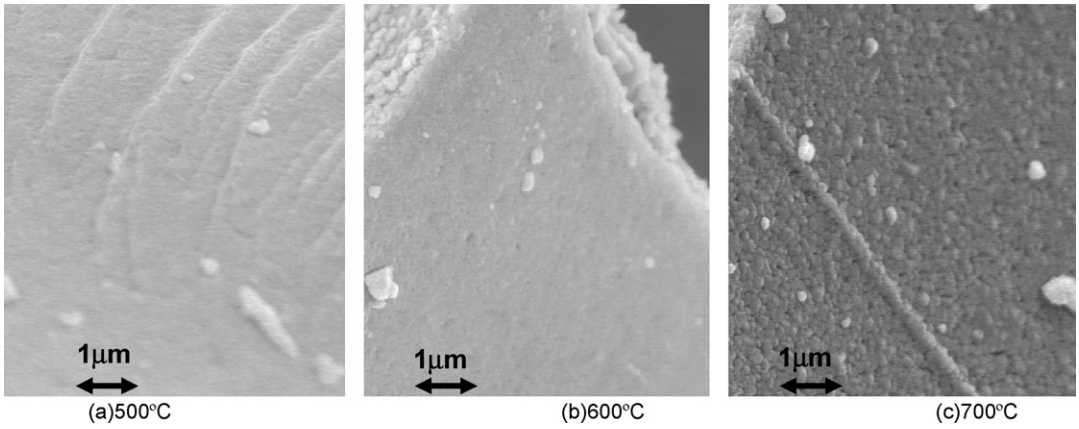


**Fig. 7.** Photographs of $WO_3$(PA) prepared at different temperature. (a) 500 °C, (b) 600 °C, and (c) 700 °C.

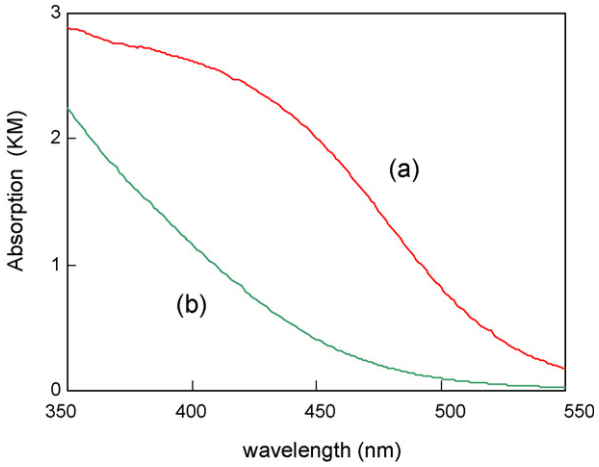


**Fig. 8.** UV–vis absorption spectra of a-PA. (a) Before and (b) after grinding with a mortar.

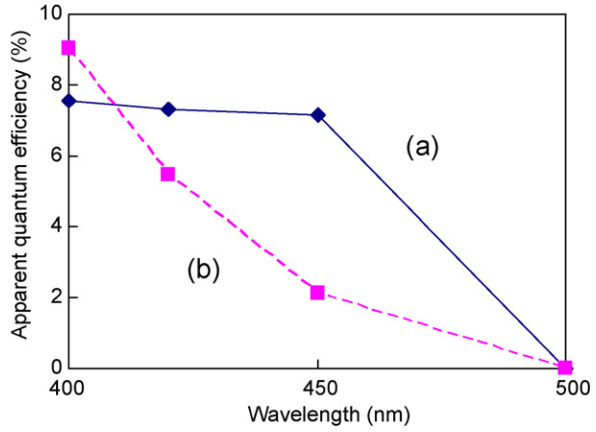


**Fig. 9.** The action spectra of the apparent quantum efficiency of $CO_2$ formation from hexane degradation using monochromatic light. (a) $WO_3$(PA) powder (calcined at 450 °C) and (b) $WO_3$(PA-g) powder after grinding.

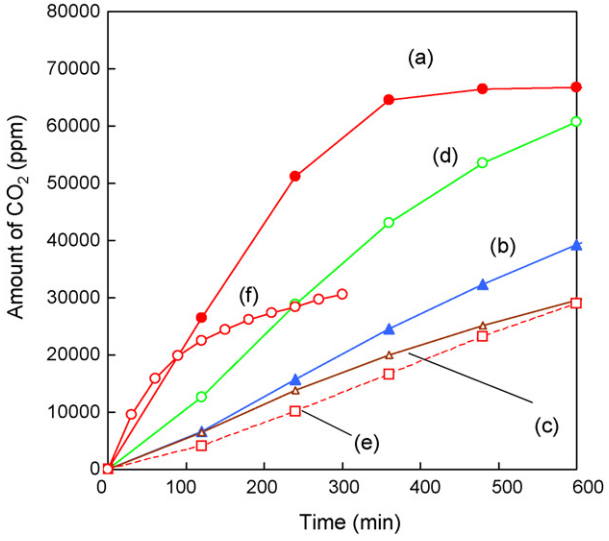


**Fig. 10.** The time course of $CO_2$ formation during the degradation of propane over $WO_3$(PA) loaded with CuO co-catalyst (0.1 wt%). Experimental conditions: Solar-simulating Xe light (1 sun) without UV cutoff filter; introduced propane: ca. 22,700 ppm. (a) $WO_3$(PA) calcined at 450 °C, (b) $WO_3$(C) calcined at 400 °C, (c) commercial $WO_3$, (d) $WO_3$(PA-g), (e) N-doped $TiO_2$, and (f) $WO_3$(PA) without CuO co-catalyst.

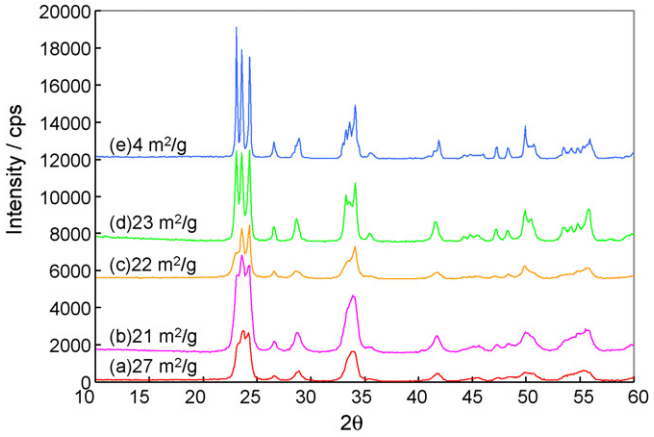


**Fig. 11.** XRD patterns of various $WO_3$ powders having similar surface areas, except commercial $WO_3$, which had a lower surface area than the others as received: (a) $WO_3$(C) calcined at 400 °C, (b) mesoporous $WO_3$ calcined at 450 °C, (c) $WO_3$ prepared by calcining $H_2WO_4$ at 400 °C, (d) $WO_3$(PA-g), and (e) commercial $WO_3$. The XRD measurement of the large grain of $WO_3$(PA) was not accurate because of the rough face on the XRD sample holder.

$WO_3$ photocatalyst without CuO could not decompose some stable intermediates such as acetic acid and formic acid [13,19]. The initial activity of $CO_2$ evolution over $WO_3$(PA) with CuO was ca. 3 and 5 times the activities over the commercial $WO_3$ with CuO and N-doped $TiO_2$ catalysts. The order of the initial activities over CuO-loaded $WO_3$ catalysts for propane degradation agreed with that over $WO_3$ catalysts for hexane degradation. The activity of $WO_3$(PA) was decreased by ca. 44% by grinding, but the activity of $WO_3$(PA-g) was much higher than the activities of other $WO_3$ powders with similar surface areas and than the activity of commercial $WO_3$. The data point (*) in Fig. 2 of the activity of $WO_3$(PA-g) for hexane degradation was also higher than those of other $WO_3$ except $WO_3$(PA). The XRD pattern of $WO_3$(PA-g) was very sharp compared with the patterns of the other homemade $WO_3$ powders with similar surface area (Fig. 11). These results suggest that the activity of the primary particle of $WO_3$(PA) and $WO_3$(PA-g) for the degradation of various organic compounds was higher than the activities of the other $WO_3$ samples because $WO_3$(PA) exhibited good crystallinity and an optimum surface area and, moreover, because $WO_3$(PA) had a more efficient light harvesting ability than the other samples.

The reason for the large light absorption, that is, the small light reflection, of $WO_3$(PA) is not clear, but some possibilities are discussed. Some methods are known to decrease reflection [25–29]. For example, a large difference in refractive index at the interface causes a large reflection; therefore, the gradient surface structures of refractive index using a multi-layer of various materials with different refractive index or a control of surface roughness and porosity are very effective [25,26]. Photonic crystals having a three-dimensional periodic structure are also effective for optical confinement [27], but this effect can be excluded because any periodic structure of a few hundred nanometers could not be found in $WO_3$(PA). For solar cell thin films, macroscopic optical confinement by means of increasing light path length through a backscattering layer structure has been reported [28,29]. The most notable characteristic of $WO_3$(PA) powder was its smooth surface: the roughness of the surface was less than the size of the primary particles (<40 nm). The surface of a-PA was also very smooth. In contrast, the surface morphologies of all the other samples investigated here were very rough, more than a few hundred nanometers, and those samples contained large aggregates formed by the primary particles (Fig. 12). For example, the size of the primary particles of $WO_3$(C) observed by SEM was almost same as

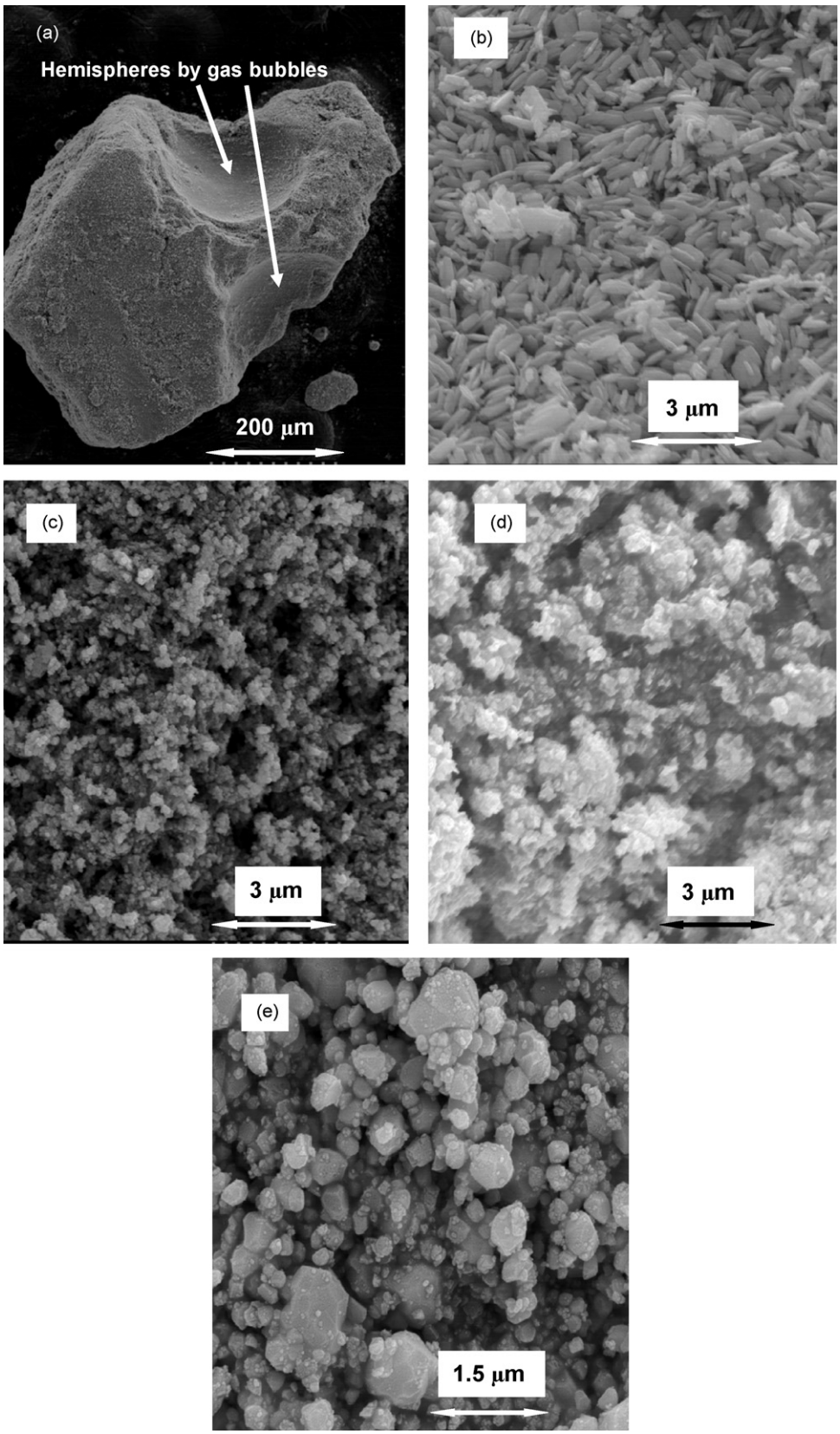


**Fig. 12.** SEM photographs of various $WO_3$. (a) $WO_3$(C) at 400 °C at low magnification, (b) $WO_3$(C) at 400 °C at high magnification, (c) mesoporous $WO_3$ at 450 °C, (d) $WO_3$ prepared by calcining $H_2WO_4$ at 400 °C, and (e) commercial $WO_3$.

that of $WO_3$(PA), but aggregates of the secondary structure having a distorted spindle shape (800 nm × 300 nm × 100 nm) were observed at the surface as well as inside the $WO_3$(C) powder (Fig. 12a and b). Therefore, the surface morphology of the $WO_3$(C) powder was very rough. The surface of the $WO_3$(PA-g) powder (Fig. 4g) was also rougher than a few hundred nanometers, owing to random aggregates of the primary particles. The diffuse reflection is known to reach a maximum when the particle size

of aggregates or surface roughness is similar to the incident light wavelength, because of Mie scattering. Therefore, powders with surface roughnesses of a few hundred nanometers showed a large light reflection. Moreover, the surface porosity of the $WO_3$(PA) powder might also have contributed to the decreased light reflection, because the apparent density and the apparent refractive index decreased and the large difference of refractive index at the interface against air was reduced. The reflection might be reduced at smooth and porous surface, like $WO_3$(PA). Additionally, some structures beneath the transparent surface of $WO_3$(PA) were observed with the optical microscope (Fig. 4a). This result suggests that these structures, such as strong aggregates and hollows, had different refractive indices, and the incident light was refracted at the interface of these structures within the $WO_3$ matrix. Therefore, the light absorption might be improved by lengthening the light path, owing to the duplicating of refraction and diffusion inside the $WO_3$(PA) powder.

## 4. Summary

The photocatalytic activity toward some VOCs degradation was investigated over $WO_3$ photocatalysts prepared by various methods, and $WO_3$(PA) prepared by amorphous peroxo-tungstic acid showed the highest activity among all $WO_3$ photocatalysts. The $CO_2$ evolution rate for hexane oxidation over $WO_3$(PA) was ca. 6 times higher than that over commercial $WO_3$. The optimum surface area was around 15–30 $m^2/g$ for each preparation method. CuO-loaded $WO_3$(PA) also showed high activities for the complete oxidation of various organic compounds to $CO_2$. The activity of $WO_3$(PA) with high surface area and good crystallinity was higher than the activities of various $WO_3$, and $WO_3$(PA) powder had the additional advantage of efficient light harvesting ability in the visible light region. We speculated that the light absorption of $WO_3$(PA) powder was improved relative to that of the other samples because of a decrease in surface reflection at the smooth and porous surface of $WO_3$(PA) and because of its increased light path length.

## Acknowledgement

This research was supported by the Project to Create Photocatalyst Industry for Recycling-oriented Society from the New Energy and Industrial Technology Development Organization (NEDO).

## References

[1] R. Asahi, T. Morikawa, T. Ohwaki, K. Aoki, Y. Taga, Science 293 (2001) 269.
[2] Y. Irokawa, T. Morikawa, K. Aoki, S. Kosaka, T. Ohwaki, Y. Taga, Phys. Chem. Chem. Phys. 8 (2006) 1116.
[3] T. Ohno, T. Mitsui, M. Matsumura, Chem. Lett. 32 (2003) 364.
[4] H. Irie, Y. Watanabe, K. Hashimoto, Chem. Lett. 32 (2003) 772.
[5] A. Di Paola, L. Palmisano, V. Augugliaro, Catal. Today 58 (2000) 141.
[6] K.G. Kim, E.D. Jeong, P.H. Borse, S. Jeon, K. Yong, J.S. Lee, W. Li, S.H. Oh, Appl. Phys. Lett. 89 (2006) 064103.
[7] K. Vinodgopal, I. Bedja, S. Hotchandani, P.V. Kamat, Langmuir 10 (1994) 1767.
[8] A. Sclafani, L. Palmisano, G. Marcí, A.M. Venezia, Sol. Energy Mater. Sol. Cells 51 (1998) 203.
[9] T. Nosaka, M. Yoshitake, S. Ogawa, J. Yotsuya, H. Matsuoka, Abstract of Third Annual Conference of the Vacuum Society of Japan (Kansai Branch), 1999, p. 13.
[10] R. Abe, H. Takami, N. Murakami, B. Ohtani, J. Am. Chem. Soc. 130 (2008) 7790.
[11] T. Arai, M. Horiguchi, M. Yanagida, T. Gunji, H. Sugihara, K. Sayama, Chem. Commun. (2008) 5565.
[12] T. Arai, M. Yanagida, Y. Konishi, Y. Iwasaki, H. Sugihara, K. Sayama, J. Phys. Chem. C 111 (2007) 7574.
[13] T. Arai, M. Yanagida, Y. Konishi, Y. Iwasaki, H. Sugihara, K. Sayama, Cat. Commun. 9 (2008) 1254.
[14] T. Arai, M. Yanagida, Y. Konishi, H. Sugihara, K. Sayama, Electrochemistry 76 (2008) 128.
[15] T. Arai, M. Yanagida, Y. Konishi, A. Ikura, Y. Iwasaki, H. Sugihara, K. Sayama, Appl. Catal. B: Environ. 84 (2008) 42.
[16] H. Irie, S. Miura, K. Kamiya, K. Hashimoto, Chem. Phys. Lett. 457 (2008) 202.
[17] Z. Zhao, M. Miyauchi, Angewandte Chemie Int. Ed. 47 (2008) 7051.
[18] M. Sadakane, K. Sasaki, H. Kunioku, B. Ohtani, W. Ueda, R. Abe, Chem. Commun. (2008) 6552.
[19] T. Arai, M. Horiguchi, M. Yanagida, T. Gunji, H. Sugihara, K. Sayama, J. Phys. Chem. C 113 (2009) 6602–6609.
[20] B. Pecquenard, S. Castro-Garcia, J. Livage, P.Y. Zavalij, M.S. Whittingham, R. Thouvenot, Chem. Mater. 10 (1998) 1882.
[21] K. Yamanaka, H. Okamoto, H. Kidou, T. Kudo, Jpn. J. Appl. Phys. 1 25 (1986) 1420.
[22] W.H. Lai, J. Shieh, L.G. Teoh, I.M. Hung, C.S. Liao, M.H. Hon, J. Alloys Compd. 396 (2005) 295.
[23] K. Sayama, K. Mukasa, R. Abe, Y. Abe, H. Arakawa, Chem. Commun. (2001) 2416.
[24] G. Bamwenda, T. Uesigi, Y. Abe, K. Sayama, H. Arakawa, Appl. Catal. A: Gen. 205 (2001) 117.
[25] H. Kikuta, H. Toyota, W.J. Yu, Opt. Rev. 10 (2003) 63.
[26] A. Mizutani, H. Kikuta, K. Iwata, H. Toyata, J. Opt. Soc. Am., A 19 (2002) 1346.
[27] T. Sumida, Y. Wada, T. Kitamura, S. Yanagida, Chem. Lett. (2002) 180.
[28] Y. Chiba, Y.A. Islam, A.Y. Watanabe, R. Komiya, N. Koide, L. Han, Jpn. J. Appl. Phys., Part 2 45 (2006) L638.
[29] A. Usami, Sol. Energy Mater. Sol. Cells 64 (2000) 73.